POLITECNICO DI TORINO
Repository ISTITUZIONALE

Cost Effective PCB Gap Waveguide Based on Broken Glide Symmetry

Original
Cost Effective PCB Gap Waveguide Based on Broken Glide Symmetry / Aktas, K., Petek, M., Tolin, E., Bruni, S., Vipiana, F.. - (2025), pp. 1-4. (19th European Conference on Antennas and Propagation (EuCAP 2025) Stockholm (Swe) 30 March 2025 - 04 April 2025) [10.23919/EuCAP63536.2025.10999204].

Availability:
This version is available at: 11583/3015755 since: 2026-09-22T10:33:48Z

Publisher:
IEEE

Published
DOI:10.23919/EuCAP63536.2025.10999204

Terms of use:

This article is made available under terms and conditions as specified in the corresponding bibliographic description in the repository

Publisher copyright
IEEE postprint/Author's Accepted Manuscript

©2025 IEEE. Personal use of this material is permitted. Permission from IEEE must be obtained for all other uses, in any current or future media, including reprinting/republishing this material for advertising or promotional purposes, creating new collecting works, for resale or lists, or reuse of any copyrighted component of this work in other works.

(Article begins on next page)

12 November 2026

Cost Effective PCB Gap Waveguide Based on Broken Glide Symmetry

Kaan Aktas*, Martin Petek*, Enrico Tolin†, Simona Bruni†, Francesca Vipiana*
*Dept. of Electronics and Telecommunications, Politecnico di Torino, 10129 Torino, Italy, kaan.aktas@polito.it
†Antenna and EM Modelling, IMST GmbH, 47475 Kamp-Lintfort, Germany, simona.bruni,enrico.tolin@imst.de

***Abstract*—Gap waveguides can provide a cost-effective and low-loss solution for high frequency transmission line technologies. This paper introduces a novel electromagnetic bandgap structure for a gap waveguide operating across the entire E band, targeting automotive radar applications. The proposed concept is compatible with cost-effective FR4-based printed circuit boards, utilizing substrate-integrated hole unit cells. Broken glide-symmetric geometry is adopted in the proposed approach to reach wider stopbands and greater adaptability for larger gap sizes. The final design achieves an average transmission loss of 0.1 dB/cm within the $76-81$ GHz frequency band.**

***Index Terms*—EBG, gap waveguides, glide symmetry, PCB technology, periodic structures, substrate integrated hole unit cells.**

I. Introduction

Autonomous driving is an emerging megatrend in automobile industry that incorporates large bandwidth radar systems to detect surrounding objects with high resolution. The recent allocation of the $76-81$ GHz band for these radars in Europe and the United States has replaced the traditional 24 GHz ultra-wideband. This new spectrum not only allows to distinguish closely spaced objects, but offers also a higher precision in their velocity measurements [1], [2].

However, signal transmission from the microchip to the antenna using hollow waveguide or microstripline technologies suffers from transmission losses at these frequencies. The reliability of metallic hollow waveguides decreases due to the increased risk of gap forming between the joined metal parts, causing leakage. Whereas, microstrip lines, although advantageous due to their low cost, experience dielectric and radiation losses [3]. Instead, gap waveguides, using electromagnetic bandgap (EBG) structures, offer a promising alternative. Their stopband property effectively prevents leakage, and the majority of the waves propagate through the hollow cavity of the waveguide channel [4].

It has been demonstrated that EBGs based on glide symmetry can achieve wider bandgaps. These periodic structures possess higher symmetries, remaining invariant under both reflection and translation by half a period. Examples of such structures include pins, holey, or corrugated metallic surfaces [5]. As explored in [6], breaking the glide symmetry can further manipulate the dispersion diagram by shifting the modes that create bandgaps to different frequency ranges.

The automotive market requires solutions which are cost effective and easy to manufacture in large volume. Therefore,

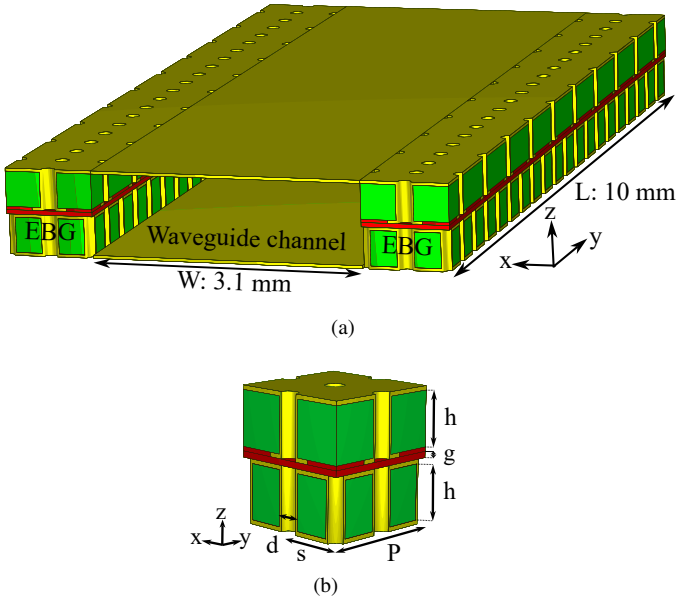


Fig. 1. (a) Gap waveguide featuring an EBG row on each side and a parallel plate waveguide channel with air cavity. (b) Broken glide-symmetric unit cell of the EBG repeated along y axis. The materials are annealed copper (yellow) and FR4 (red and green). The geometrical dimensions are $W = 3.1$ mm, $L = 10$ mm, width and length of waveguide channel, respectively; $h = 450\,\mu$m substrate height, $g = 50\,\mu$m gap height, $P = 1$ mm cell-size period; d is the via diameter and s the via to via distance.

to enhance cost-effectiveness, printed circuit board (PCB) technology can be employed to imitate metallic structures using via holes and patches. These are known as substrate-integrated hole (SIH) unit cells [7]. Unlike substrate-integrated waveguides (SIW) [8], which rely on closely spaced through vias to prevent leakage, SIH approach leverages the stopband properties of unit cells. Previous studies in [9] and [10] have demonstrated that these cells can create a stopband, making them promising for this application. However, the glide-symmetric implementation in [9] operate at frequencies below E band. Whereas, [10] is a non glide-symmetric solution that can reach $83-100$ GHz stopband, but designed with a $350\,\mu$m gap filled with air which poses challenges for multi-layer PCB manufacturing.

Therefore, to address the challenge of feeding the antenna from the microchip, this paper introduces a novel gap waveguide structure shown in Fig. 1a, operating across the entire E band, i.e. $60-90$ GHz. The proposed design is suitable

for a multilayer FR4 PCB technology and employs SIH unit cells that breaks the glide symmetry (see Fig. 1b) to widen the stopband.

II. Unit Cell Design

This section presents the fundamental SIH unit cell structure based on the common design parameters shown in Fig. 1b. Subsequently, it compares the performance of glide-symmetric and broken glide-symmetric configurations depicted in Fig. 2. These designs are engineered to create a stopband that includes the $76-81$ GHz frequency range and covers the entire irreducible Brillouin zone. Dispersion diagram simulations in Figs. 3 and 4 are performed with an eigenvalue solver using periodic boundary conditions on x and y directions and perfect electric conductor (PEC) on z axis.

Each unit cell features top and bottom components, each of which is a substrate of height, h, coated with etched copper layers. The vias are placed as a cross on the top, and 2D glide symmetry is applied at the bottom, meaning that mirror image of the top part is shifted by half a period P on x and y directions [5]. Vias at the edges are shared between adjacent unit cells to reduce via consumption. To minimize the radiation losses through the spacing between via holes, the via diameter d and the spacing distance s are determined according to [8]. The top and bottom parts are separated by a central substrate of thickness $g = 50\,\mu$m, the thinnest commercially available option [11]. All cells have periodicity $P = 1$ mm, and utilize the default FR4 material ($\epsilon_r = 4.3$ and $\tan\delta = 0.025$). Regarding all these fixed parameters, the unit cell height, h, is used to adjust the stopband for the desired band.

The glide-symmetric version in Fig. 2a has a height $h = 200\,\mu$m, resulting in a central frequency of 79.8 GHz with a 31.4% fractional bandwidth between modes 4 and 5, as shown in Fig. 3a. To break the symmetry, the via pads in glide-symmetric design are connected with a copper strip of width r. It is placed at the bottom part only, as shown in Fig. 2b, creating a square aperture in the inner copper layer. This modification forms a stopband between mode 3 and 4 in the dispersion diagram (Fig. 3b). The former experience a decrease in frequency, while modes 4 and 5 shift to even higher frequencies compared to the glide-symmetric version. This leads to a 64.4% fractional bandwidth with a mid bandgap frequency at 83.8 GHz while maintaining the same dimensions as in glide symmetry.

Smaller gap size, g, increases the stopband as depicted in Fig. 4. That is why the thinnest substrate available is used in our analyses to test the stopband band capability of unit cells. However, larger gaps leads to reduced manufacturing costs and improved precision. In Fig. 4, we notice that this new cell becomes much more robust and adaptable to manufacturing process enduring a stopband despite bigger gap sizes.

Furthermore, by increasing the height, h, of the broken glide-symmetric cell to $450\,\mu$m (Fig. 2c), the stopband can be expanded. This enhancement yields a 98.7% fractional bandwidth centered at 72.7 GHz (Fig. 3b), encompassing not only the E band but also the U ($40-60$ GHz) and W ($75-110$ GHz) bands.

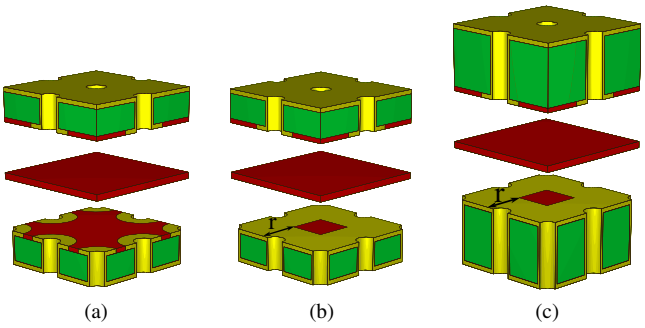


Fig. 2. Three unit cell configurations visualised with individual parts separated: (a) a glide-symmetric unit cell with $h = 200\,\mu$m, (b) a broken glide-symmetric configuration with the same dimensions as in (a), and (c) broken glide symmetric unit cell with $h = 450\,\mu$m, as shown in Fig. 1b. The red substrate in the middle has a thickness $g = 50\,\mu$m; r is the width of inner copper layer to break the symmetry.

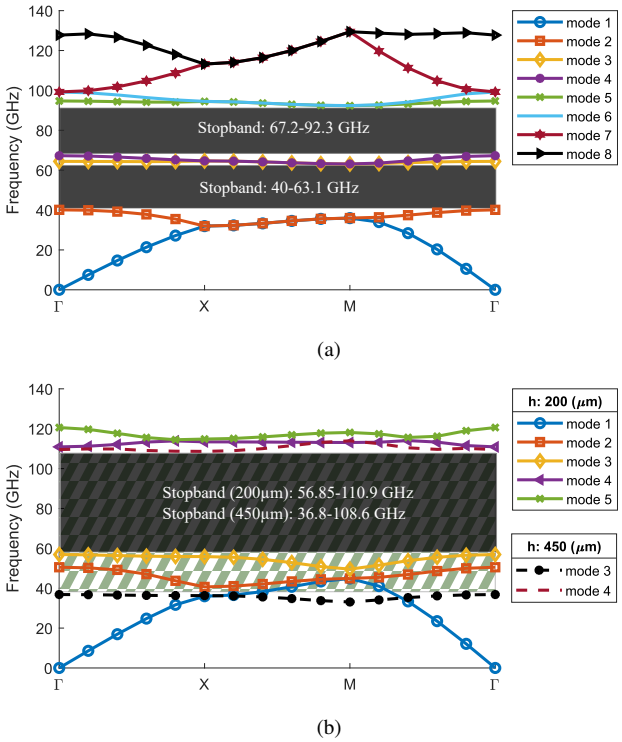


Fig. 3. Dispersion diagrams of glide symmetric (a) and broken glide symmetric (b) unit cells in Fig. 2. Stopbands of Fig. 2a and 2b are indicated with solid black region. Whereas for Fig. 2c gray stripes are used. Only the modes contributing to the stopband are displayed for the latter unit cell.

Overall, broken symmetry gives more flexibility in the gap waveguide design as well as it can provide a high stopband performance in any propagation direction. Unlike previous research [6] where breaking the symmetry resulted in a stop band divided in two, in our case it got significantly larger.

III. Gap Waveguide Design and Results

Gap waveguide design in Fig. 1a consists of two parallel plates, separated by a hollow cavity, with EBG structures

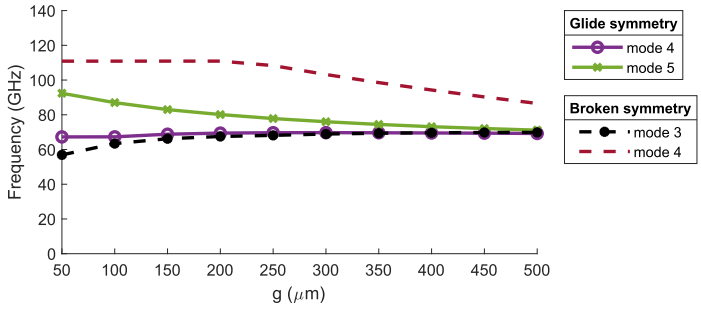


Fig. 4. The evolution of the stopband with respect to the gap size, g, in both broken glide-symmetric (Fig 2b) and glide-symmetric (Fig. 2a) unit cells of identical dimensions. Frequency values of mode 4 and 5 in glide symmetry are calculated at Γ and M points of the Brillouin zone, respectively. For broken glide symmetry, it is at Γ only. Their stopbands are defined at these points according to Fig. 3.

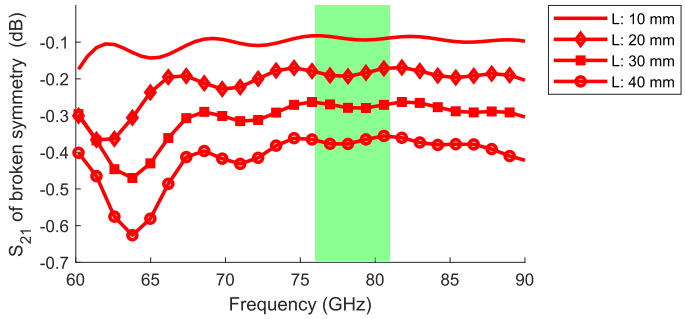


Fig. 5. Transmission coefficient of the gap waveguide (Fig 1a) based on broken glide symmetry for lengths, L, ranging from 10 to 40 mm. The $76-81$ GHz band is emphasized in green.

placed on either side. These EBGs are formed by repeating one row of either a glide-symmetric unit cell in Fig. 2a or a broken glide-symmetric unit cell in Fig. 2c along the direction of wave propagation. Due to space constraints in automotive applications and to reduce computational time, we limited the EBG length to 10 unit cell periods in our analysis. As expected, longer EBGs increase transmission losses, as can be noticed in Fig. 5.

Simulations are done in E band frequency range using a time domain solver and include material losses. TE_{10} wave is excited with a waveguide port placed at the air cavity with 3.1 mm width (WR12 waveguide) to ensure a cutoff frequency below E band. The height matches with unit cell's height without outer copper layers.

Results of gap waveguide based on broken glide symmetry presented in Fig. 6 aligns with predictions in the dispersion diagram. It achieves a transmission coefficient exceeding -0.1 dB throughout the $76-81$ GHz band despite lossy materials and only one row of EBG. Furthermore, it remains above -0.2 dB throughout the E band with a reflection coefficient below -25 dB. Its transmission losses are calculated by averaging the difference between transmission coefficients for various lengths depicted in Fig. 5. They are 0.092 dB/cm for $76-81$ GHz frequency range and 0.105 dB/cm for E band.

To highlight the presented solution performance, we compare losses per unit length with similar metallic waveguide and SIW structures. Therefore, the same calculations are done for a hollow WR12 waveguide constructed from $35\,\mu$m thick annealed copper, a standard thickness used in PCBs. Additionally, a SIW waveguide is realized in standard FR4 material, with WR12 dimensions and equally spaced via rows, each with a diameter of $200\,\mu$m and separated by $400\,\mu$m.

This study shows that the waveguide achieved a loss of 0.02 dB/cm at $76-81$ GHz band. Consequently, for shorter lengths, the gap waveguide performance closely approaches to an actual waveguide. On the other hand, the SIW was resulting in a loss of 3.08 dB/cm at $76-81$ GHz. Due to FR4 high loss tangent and permittivity, SIW has greater transmission losses

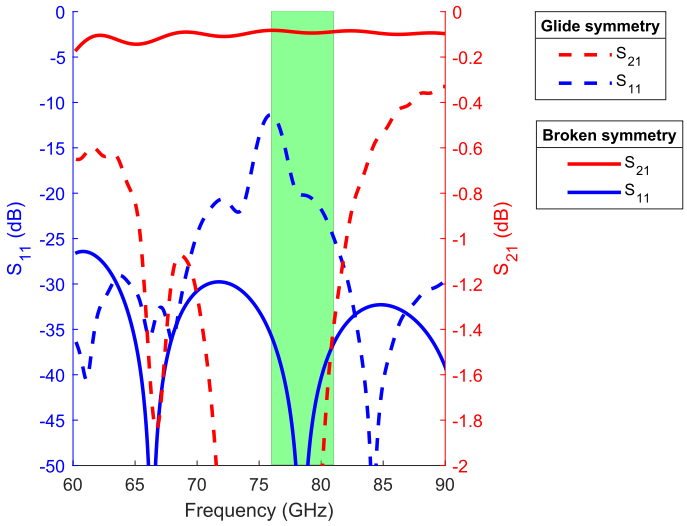


Fig. 6. Transmission (S_{21}) and reflection (S_{11}) coefficient of the gap waveguide in Fig 1a with $L = 10$ mm using glide symmetric (Fig. 2a) and broken glide symmetric (Fig. 2c) configurations. The $76-81$ GHz frequency range is highlighted in green.

compared to the other two designs.

Regarding glide symmetric version, in Fig. 6 we observe narrowband regions with S21 values higher than -1 dB. Despite low reflections, transmission coefficient drops below -1 dB at 66.5 GHz. This indicates that the EBG cannot fully suppress propagation and leads to leakage, which aligns with its dispersion diagram. Nevertheless, the optimal performance occurs at 89 GHz, deviating from the intended design range of $76-81$ GHz due to reflections around 74 GHz.

Overall, the proposed gap waveguide solution showcases the potential of SIH cells for achieving higher operating frequencies. We can demonstrate that broken glide symmetry outperforms the glide symmetric version with transmission coefficient values over -0.2 dB across the entire E band. Moreover, it exhibits significantly lower transmission losses than SIW with its air-filled cavity and achieves a performance comparable to a copper hollow waveguide with 0.072 dB/cm

difference, despite the use of standard FR4 material as basis material.

IV. Conclusion

In this paper, we have demonstrated that reaching E band frequencies is possible with an FR4 PCB gap waveguide structure to address the current demand in automative radar technology. Despite using lossy materials, the simulations of our proposed gap waveguide has shown a transmission loss of $0.1\,\mathrm{dB/cm}$ across the $76-81\,\mathrm{GHz}$ band.

Furthermore, we have shown that EBGs based on SIH unit cells with broken glide symmetry have better performance, allowing them to suppress all modes across U, E and W bands, regardless of propagation direction. These cells are also capable of maintaining a stopband for gap sizes more than $500\,\mu\mathrm{m}$ making the design adaptable to manufacturing.

Therefore, this innovative concept provides a cost-effective solution for high-frequency applications offering an alternative to other transmission line approaches. Its performance makes it a promising candidate to provide effective structures for automotive radar technology.

Acknowledgment

This publication is based upon work supported by the Horizon Europe Research and Innovation Program and UKRI under the GENIUS Project, Marie Skłodowska-Curie Grant under Agreement 101072560. It is also supported by Unite! – University Network for Innovation, Technology and Engineering.

References

[1] IEEE, "Heterogeneous Integration Roadmap, Chapter 5: Automotive," IEEE Electronics Packaging Society (EPS), Tech. Rep., 2021. [Online]. Available: https://eps.ieee.org/images/files/HIR_2021/ch05_automotive.pdf

[2] K. Ramasubramanian and K. Ramaiah, "Moving from Legacy 24 GHz to State-of-the-Art 77-GHz Radar," *ATZelektronik worldwide*, vol. 13, no. 3, pp. 46–49, Jun 2018. [Online]. Available: https://doi.org/10.1007/s38314-018-0029-6

[3] W. Y. Yong, A. Vosoogh, A. Bagheri, C. Van De Ven, A. Hadaddi, and A. A. Glazunov, "An Overview of Recent Development of the Gap-Waveguide Technology for mmWave and Sub-THz Applications," *IEEE Access*, vol. 11, pp. 69 378–69 400, 2023.

[4] J.-L. A. Lijarcio, A. Vosoogh, C. Bencivenni, and A. U. Zaman, "Low-Cost Center-Fed Slot Array Based on Gap Waveguide MLW Coaxial Line Technology for E-Band Automotive Radar," *IEEE Transactions on Antennas and Propagation*, vol. 72, no. 7, pp. 5674–5681, 2024.

[5] O. Quevedo-Teruel, Q. Chen, F. Mesa, N. J. G. Fonseca, and G. Valerio, "On the Benefits of Glide Symmetries for Microwave Devices," *IEEE Journal of Microwaves*, vol. 1, no. 1, pp. 457–469, Jan 2021.

[6] P. Padilla, A. Palomares-Caballero, A. Alex-Amor, J. Valenzuela-valdés, J. M. Fernández-González, and O. Quevedo-Teruel, "Broken Glide-Symmetric Holey Structures for Bandgap Selection in Gap-Waveguide Technology," *IEEE Microwave and Wireless Components Letters*, vol. 29, no. 5, pp. 327–329, 2019.

[7] Q. Chen, F. Giusti, G. Valerio, F. Mesa, and O. Quevedo-Teruel, "Anisotropic glide-symmetric substrate-integrated-holey metasurface for a compressed ultrawideband Luneburg lens," *Applied Physics Letters*, vol. 118, no. 8, 2021.

[8] M. Bozzi, A. Georgiadis, and K. Wu, "Review of substrate-integrated waveguide circuits and antennas," *IET Microwaves, Antennas & Propagation*, vol. 5, no. 8, pp. 909–920, 2011.

[9] B. Fischer, J. Sarrazin, and G. Valerio, "Glide-Symmetric Reconfigurable Substrate-Integrated Holey Waveguide," in *2024 18th European Conference on Antennas and Propagation (EuCAP)*, 2024, pp. 1–4.

[10] F. Ghasemifard, F. Mesa, G. Valerio, and O. Quevedo-Teruel, "Propagation characteristics in substrate integrated holey metasurfaces," in *2020 14th European Conference on Antennas and Propagation (EuCAP)*. IEEE, 2020, pp. 1–4.

[11] Isola. (2024) PCB Laminate and Prepreg Materials. [Online]. Available: https://www.isola-group.com/pcb-laminates-prepreg/